AGU100 ADVANCING EARTH AND SPACE SCIENCE

Geophysical Research Letters

RESEARCH LETTER
10.1029/2020GL086958

Key Points:
- THEMIS multicomponent wave data on VLF chorus in the source region are analyzed
- Opposite Poynting flux directions in shifted frequency bands are observed
- Theoretical explanation based on the backward wave oscillator model is proposed

Supporting Information:
- Supporting Information S1

Correspondence to:
A. G. Demekhov,
andrei@ipfran.ru

Citation:
Demekhov, A. G., Taubenschuss, U., Hanzelka, M., & Santolík, O. (2020). Frequency dependence of very low frequency chorus
Poynting flux in the source region: THEMIS observations and a model. *Geophysical Research Letters*, *47*, e2020GL086958. https://doi.org/10.1029/2020GL086958

Received 2 JAN 2020
Accepted 7 MAR 2020
Accepted article online 11 MAR 2020

Frequency Dependence of Very Low Frequency Chorus Poynting Flux in the Source Region: THEMIS Observations and a Model

A. G. Demekhov[1,2], U. Taubenschuss[3], M. Hanzelka[3,4], and O. Santolík[3,4]

[1]Polar Geophysical Institute, Apatity, Russia, [2]Institute of Applied Physics of the Russian Academy of Sciences, Nizhny Novgorod, Russia, [3]Department of Space Physics, Institute of Atmospheric Physics, Czech Academy of Sciences, Prague, Czechia, [4]Faculty of Mathematics and Physics, Charles University in Prague, Prague, Czechia

Abstract Using Poynting vector measurements of whistler mode chorus emissions detected by the THEMIS spacecraft within the source region, that is, close to the magnetic field minimum, we found both in individual events and statistically that chorus elements propagating equatorward had systematically higher frequencies and smaller amplitudes compared with simultaneously observed elements propagating away from the equator. We demonstrate similar features in the results of numerical simulations based on backward wave oscillator equations. It can be qualitatively explained by the nonlinear evolution of the energetic electron distribution function during wave generation. The motion of electrons from the equator is accompanied by a decrease in their velocity component along the magnetic field line due to both the adiabatic mirror force and nonlinear wave-particle interactions. Thus, the frequency of the chorus elements generated by such electrons and propagating equatorward is higher compared with the elements propagating away from the equator.

1. Introduction

Very low frequency (VLF) chorus emissions in the magnetosphere are discrete quasi-monochromatic wave packets (elements) with durations and repetition intervals as short as fractions of a second (Burtis & Helliwell, 1975; LeDocq et al., 1998; Santolík et al., 2008; Sazhin & Titova, 1978; Taylor & Gurnett, 1968; Titova et al., 2003; Tsurutani & Smith, 1977). The frequency changes rather fast within a chorus element, that is, by up to 10 kHz/s.

Chorus waves are believed to play important roles in energy transfer between different plasma species. In particular, they can accelerate energetic electrons to relativistic energies on time scales of less than a day (e.g., Reeves et al., 2013). On the other hand, chorus is responsible for the precipitation of relativistic electrons causing so called electron microbursts (Breneman et al., 2017; O'Brien et al., 2003; Oliven & Gurnett, 1968; Roeder et al., 1985).

Chorus is a very interesting nonlinear phenomenon from a theoretical point of view. Main theories of chorus generation are the backward wave oscillator (BWO) model (Demekhov & Trakhtengerts, 2005; Trakhtengerts, 1995, 1999; Trakhtengerts et al., 2004) and the nonlinear growth theory (Hikishima et al., 2009; Katoh & Omura, 2006; Omura et al., 2008). The existing theories and numerical models (see also Tao et al., 2014; Kuzichev et al., 2019) can successfully explain the formation of individual elements, that is, yield correct values of wave amplitudes, pulse durations, and frequency drift rates. The BWO model can also reproduce the succession of elements (Demekhov et al., 2017).

Modern spacecraft data include high-resolution multicomponent wave measurements and, thus, provide an opportunity to test details of the wave evolution in the generation region and compare the observed characteristics with the modeling results. In this paper, we discuss results of wideband measurements of chorus emissions detected by the THEMIS spacecraft in close vicinity of the geomagnetic field minimum, that is, inside their generation region.

THEMIS data presented in section 2 demonstrate a specific feature of chorus elements in the near-equatorial region: chorus wave packets propagating in opposite directions have slightly different frequencies and amplitudes. This feature has been first reported by Agapitov et al. (2011) who explained it as a signature of

reflected chorus emissions, which were generated at lower L shells and undergone an outward shift during the wave propagation in the magnetosphere, reflection from lower hybrid resonance region, and which are coming back to the equatorial region. This explanation contradicted results of Parrot et al. (2004) who systematically observed opposite frequency shifts and much lower intensities of reflected chorus. Here we report new observations which disprove the hypothesis of Agapitov et al. (2011): higher-frequency and lower-amplitude chorus elements systematically propagate toward the equator. We propose an explanation based on nonlinear evolution of the wave spectra in the generation region. Using a self-consistent numerical model of chorus generation developed by Demekhov and Trakhtengerts (2005), which is based on the BWO mechanism, we simulate one of the observed THEMIS events. These simulation results are presented in section 3. We show that the simulated chorus bursts, similarly to the observed ones, have a higher frequency and lower amplitude when they propagate toward the equator than those propagating from the equator. In section 5 we summarize our findings.

2. THEMIS Observations

2.1. Instruments and Data

The THEMIS mission was launched in early 2007 for studies of substorm and radiation belt dynamics (Angelopoulos, 2008). It consists of five spacecraft carrying identical instruments, of which we use data from four instruments. The external quasistatic magnetic field is measured by a fluxgate magnetometer (Auster et al., 2008). Magnetic and electric fields of waves are measured, respectively, by a triaxial search coil magnetometer (Le Contel et al., 2008) and the Electric Field Instrument (Bonnell et al., 2008). The latter also provides an estimation of the cold electron density from the spacecraft floating potential (Li et al., 2010). Electrons in the energy range of 7 eV to 30 keV are measured by the Electrostatic Analyzer (McFadden et al., 2008) with a time resolution of 3 s.

We use data from the "wave-burst" mode, which samples magnetic and electric waveforms at a sampling rate of 8192 Hz. This high-resolution mode of observation is activated about 10–20 times per orbit due to limitations from data transfer rates and onboard storage. Each burst mode snapshot lasts for 8 s. These measurements enable polarization analysis of whistler mode chorus with the necessary high time-frequency resolution. Waveforms are subject to spectral analysis yielding autocorrelation and cross-correlation products, which are compiled to a complex spectral matrix. The spectral matrix is analyzed via singular value decomposition (Santolík et al., 2003; Taubenschuss & Santolík, 2019). Singular values and singular vectors contain the full information on the polarization of measured waves.

2.2. Characteristics of the Events

Chorus elements with oppositely propagating Poynting flux inside the source region exhibit peculiar differences in frequency and intensity depending on their propagation to or from the B_0-minimum along the field line (referred to as the magnetic equator throughout this paper). This phenomenon was first reported from an observational point of view for two events by Taubenschuss et al. (2017). By examining data from THEMIS-A, THEMIS-D, and THEMIS-E for the first 5 years of the THEMIS mission (2007–2012), we have identified 156 events, most of which are recorded just a few thousand kilometers from the magnetic equator, that is, inside the expected chorus generation region (LeDocq et al., 1998; Santolík et al., 2005; Taubenschuss et al., 2016). The position of the magnetic equator is determined from the Tsyganenko-TS05 model (Tsyganenko & Sitnov, 2005) since $\nabla(B_0)$ along the field line is unknown from single-spacecraft measurements. As model input parameters for the solar wind we use data from the ACE and Wind satellites (Lepping et al., 1995; Lin et al., 1995; McComas et al., 1998; Smith et al., 1998). Events were identified manually ("by eye") by browsing through all dynamic spectrograms generated from 8-s burst mode snapshots. The term "event" is used for a snapshot with the following features: (a) visibility of chorus emission with either rising or falling-tone structure, (b) observed between the lower hybrid frequency and the local electron cyclotron frequency, (c) right-handed polarization of the magnetic field, and, most importantly, (d) presence of opposite Poynting vector directions for successive chorus elements.

In the present paper, we analyze three individual cases and study the phenomenon statistically. Respective L shells are between 5 and 12, and observations belong predominantly to the morningside ($2hr < \mathrm{MLT} < 18$ hr, with a peak around MLT = 5 hr). Considering the small amount of 156 events from 5 years of data prevents us from performing a meaningful statistical analysis with respect to the position of observation. A strong bias toward the morning sector is most likely explained by high chorus wave intensities prevalent in this sector and by the fact that burst mode snapshots on THEMIS are mainly triggered by intense wave events.

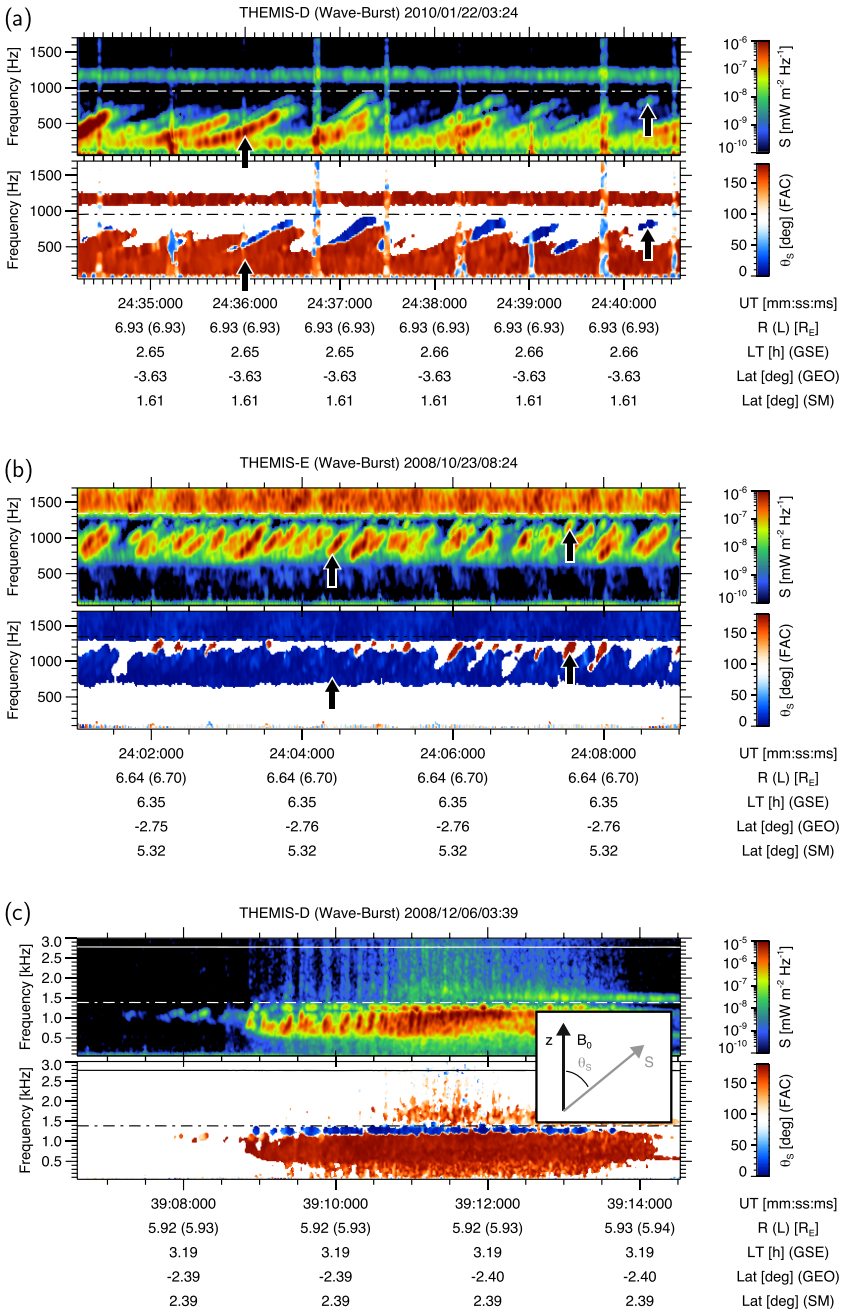

Figure 1. (a) Poynting flux S (upper panel) and polar angle θ_S (lower panel) for chorus emission observed by THEMIS-D on 22 January 2010. The dash-dotted line marks one half of the local electron cyclotron frequency. Orbital coordinates of the spacecraft are given at the bottom. Individual chorus elements marked by black arrows are analyzed in terms of wave growth rates in the supporting information. (b and c) Same as (a) but for THEMIS-E observations on 23 October 2008 and THEMIS-D observations on 6 December 2008, respectively. The values of θ_S are shown for $S > \{5 \cdot 10^{-10}; 2 \cdot 10^{-9}; 5 \cdot 10^{-9}\}$ mW/m^2 Hz^{-1} in (a), (b), and (c), respectively.

However, this does not pose a restriction to our analysis method since we focus on amplitude differences of oppositely propagating chorus elements rather than their absolute amplitudes. For our analysis, the original number of 156 events had to be reduced to 106 due to the following reasons: unclear chorus spectral features and/or frequency shifts, more than one B_0-minimum along a compressed magnetic field line (uncertainty of propagation to/from the source) and a restriction to rising tone chorus. Falling-tone chorus (five events) is excluded because there is no widely accepted formation mechanism for them, although some ideas have

been published (Demekhov, 2011; Nunn & Omura, 2012). The majority of events after cleaning belongs to lower band chorus, but upper band chorus is also included.

2.2.1. The Event of 22 January 2010

Figure 1a shows an example for a wave burst mode snapshot taken by THEMIS-D in the middle magnetosphere (L shell $\sim$ 6.9) close to the magnetic dipole equatorial plane ($LAT_{GM} \sim 1.6°$). These snapshots usually last for 8 s and cover a total frequency range of 0–4 kHz. Six cross-correlation products from electric and magnetic waveforms have been combined to calculate the Poynting vector **S**, which describes the propagation of electromagnetic energy (Santolík et al., 2010). **S** is displayed in terms of absolute value, that is, Poynting flux (upper panel), and polar direction angle θ_S (lower panel) in the field-aligned coordinate system. This system has its z axis aligned with the direction of the ambient magnetic field $\mathbf{B_0}$ (see also small inset in Figure 1c).

Intense chorus is clearly visible between 200 and 1000 Hz. The ellipticity parameter (not shown) confirms that the emission is in the right-hand-polarized whistler mode. A gap in intensity at $0.5 f_{c,e}$ ($f_{c,e}$ is the local electron cyclotron frequency) splits the emission into a lower band and an upper band. The lower band consists of a sequence of discrete elements with positive sweep rates, that is, rising tones. Their wave normal directions are nearly field aligned (not shown). A closer look at the lower panel of Figure 1a reveals that rising tones approach the spacecraft from different directions: either along the direction of $\mathbf{B_0}$ ($\theta_S \sim 0°$; shown in blue) or against the direction of $\mathbf{B_0}$ ($\theta_S \sim 180°$; shown in red). A simultaneous visibility of both propagation directions is a strong indication for THEMIS-D being inside the chorus source region during the time of observation. Besides the opposite propagation directions, there are two more differences visible. First, there is a slight shift in frequency between elements approaching along and against $\mathbf{B_0}$, and second, elements approaching along $\mathbf{B_0}$ have smaller Poynting flux. As we show below, these differences are typical for all events considered and can be explained by the BWO model for chorus generation.

2.2.2. The Event of 23 October 2008

For comparison, we present another event observed by THEMIS-E on 23 October 2008. The spacecraft is again located close to the magnetic equatorial plane and observes chorus elements with two distinct directions of the Poynting vector. These waves also propagate in the electromagnetic whistler mode with wave normal directions quasi-parallel to $\mathbf{B_0}$. However, the situation seems to be reversed in comparison to the event from THEMIS-D. As can be seen in Figure 1b, elements propagate against the direction of $\mathbf{B_0}$ (shown in red) but they still are, as in the previous case, both weaker and shifted toward higher frequencies.

2.2.3. The Event of 6 December 2008

Figure 1c shows one more example of a chorus event, recorded by THEMIS-D on 6 December 2008. Chorus elements are seen on the background of a fairly high-intensity hiss, so separate elements are not distinguished on the plot showing the Poynting vector angles. However, it is clear that the elements propagating along $\mathbf{B_0}$ have higher frequencies and lower amplitudes than the elements propagating in the opposite direction, similarly to the case of 22 January 2010.

2.2.4. Spacecraft Location Relative to the Magnetic Equator

Figures 2a–2c show results of the TS05 calculations of the magnetic field configuration for the presented events. In each plot, five field lines are shown during an interval of 30 min around the time of measurement in Figures 1a–1c, respectively. The central field lines correspond to the times of measurement. The spacecraft trajectory is indicated by a black solid line, and the gray solid line is connecting B_0-minima across field lines.

At the central field line in Figure 2a, that is, at the time of wave-burst measurement, THEMIS-D is ~1,000 km south of the B_0-minimum. For the second event, as shown in Figure 2b, calculations with the TS05-model yield that THEMIS-E is ~2,900 km north of the B_0-minimum at the time of measurement. For the third event, THEMIS-D was about 800 km south of the B_0-minimum.

Comparing Figures 2a–2c with lower panels of Figures 1a–1c, respectively, one can see that the events are in fact similar: in all three cases, the weaker elements with slightly higher frequencies propagate toward the B_0-minimum, while stronger elements with slightly lower frequencies propagate away from the equator.

Figure 2d summarizes the results for all 106 clear events analyzed. It demonstrates that the same relationship between the propagation direction, frequency, and the spacecraft location relative to the B_0-minimum holds for the majority of the events.

Another observation which we illustrate in the supporting information for brevity is that the growth rates for the oppositely propagating elements do not differ significantly from each other, unlike the wave amplitudes. This fact supports a suggestion that the observed waves originate from the same source.

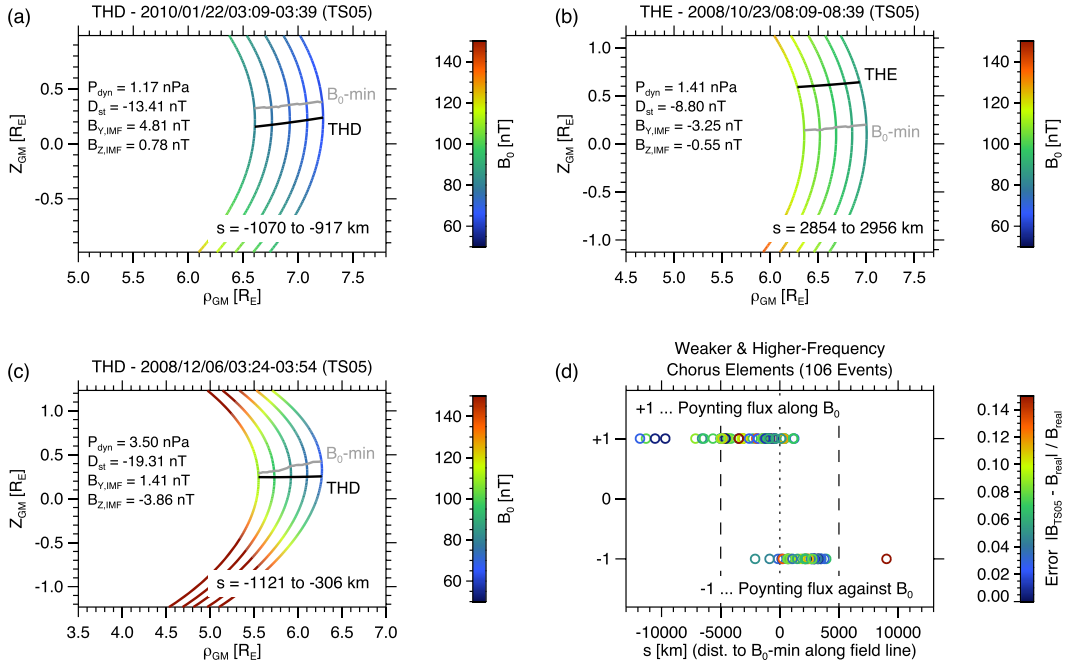

Figure 2. (a–c) Magnetic field configuration in the meridional plane of the geomagnetic coordinate system, as derived from the TS05 model for the observations presented in Figures (a) 1a, (b) 1b, and (c) 1c. The magnetic field strength B_0 along the field lines is indicated in color. B_0-minima are connected with a gray solid line. The trajectory of the spacecraft is delineated by a black solid line. Solar wind input parameters for the center time are listed as well: dynamic pressure (P_{dyn}), D_{st} index, and y and z components of the interplanetary magnetic field (in GSM coordinates). The range of distances s along the field lines between the B_0-minimum and the position of THEMIS is given at the bottom. (d) Summary plot for the position of the higher-frequency (and fainter) elements. They are plotted at +1 if the Poynting flux is directed along B_0 or −1 otherwise, as a function of the distance along the field line with respect to the B_0-minimum. Colors indicate the relative error between B_0 from the TS05 model and B_0 measured onboard THEMIS at the position of the spacecraft, providing an estimate for the accuracy of the TS05 model at the time of measurement.

In the supporting information, we also present statistics of amplitude and frequency parameters of chorus elements propagating in the opposite directions. This statistics demonstrates that the amplitude ratio from both groups is about a factor of 2–3 on average close to B_0-min and reaches 10–20 further away. The frequency difference between both chorus groups is getting smaller closer to the B_0-min.

3. Simulations Using the BWO Model

3.1. Numerical Model

We use a nonlinear self-consistent system of equations, which describes the BWO regime of the cyclotron instability. This system was derived from the initial wave and kinetic equations by Demekhov and Trakhtengerts (2005) and used by Demekhov and Trakhtengerts (2008), Demekhov (2011), and Demekhov et al. (2017). The details of the model can be found in the cited papers. We note that, in spite of being significantly simplified with respect to the initial equations, this model takes into account many important features of chorus generation.

In particular, by using the available THEMIS data on the magnetic field, plasma density, and chorus frequencies, Demekhov et al. (2017) were able to simulate the observed chorus elements and reproduce their amplitude, frequency drift, growth rate, and the characteristic interval of their repetition in a sequence. Below we present the results on the spatial dependence of the chorus spectrum, which yield an explanation of the direction-dependent frequency shift described in section 2.2.

3.2. Simulation Results

We present the simulation results for the event, described in section 2.2.3. Simulations for the other events yield similar results and are not shown here for brevity.

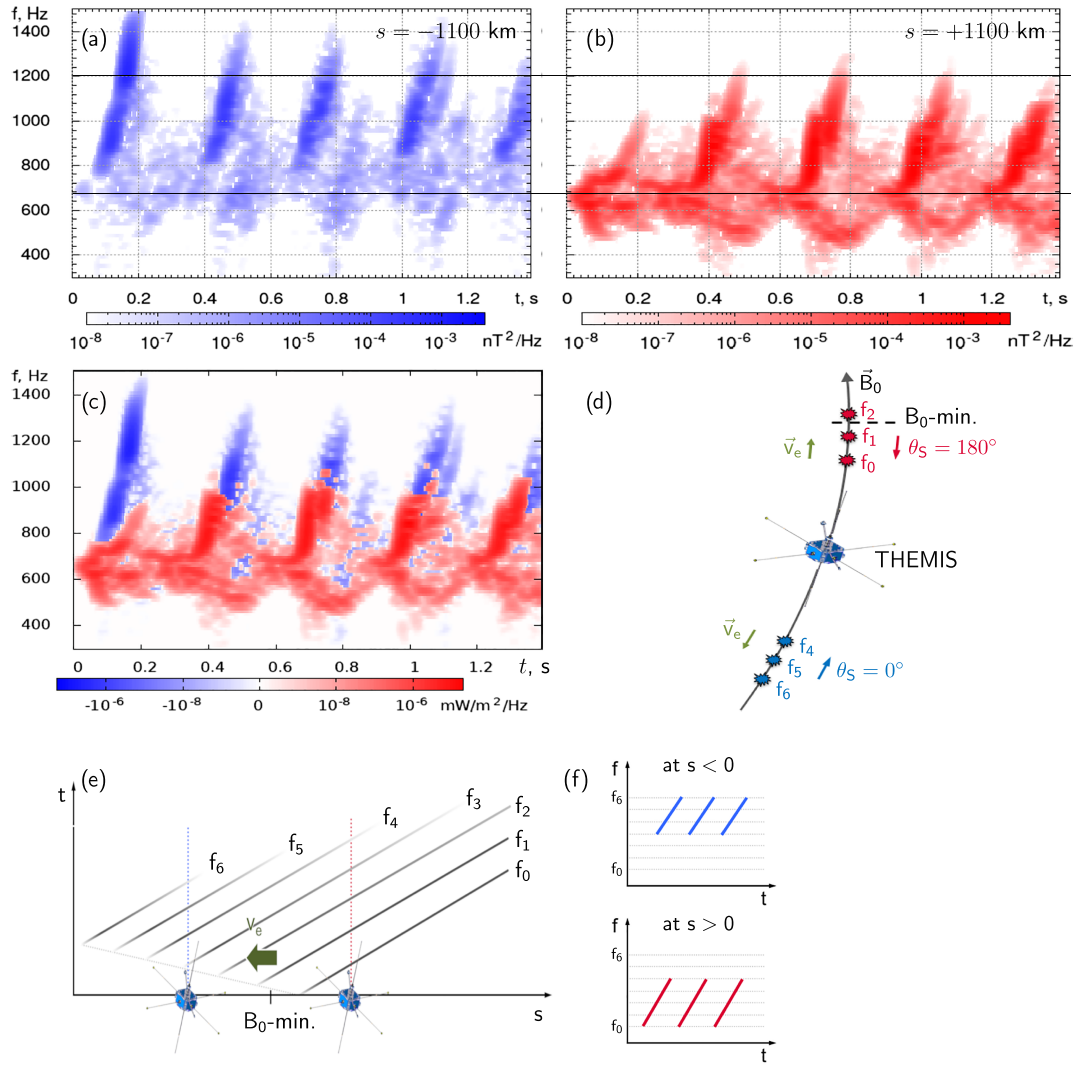

Figure 3. Simulated dynamic spectra of the VLF waves on the two opposite sides of the equator; that is, $s \approx \mp 1,100$ km for panels (a) and (b), respectively. The simulation parameters are the same as in Figure 10 in Demekhov et al. (2017). Horizontal lines are drawn to visualize the difference between the frequency bands at these two positions. Blue and red colors correspond to the waves propagating to the equator and away from it, respectively. (c) Total Poynting flux of waves propagating in both directions (to and from the equator) at $|s| \approx 1,100$ km. (d) A sketch showing two oppositely propagating wave packets ($\theta_S = 0°$ and $\theta_S = 180°$) detected by THEMIS at some distance south of the magnetic equator. The corresponding resonant electrons also have opposite directions of the parallel velocity $\vec{v}_e$. (e) A diagram showing radiation of waves with increasing frequencies f_0 to f_6 by electrons moving leftward, their propagation to the right, and detection by a spacecraft located on the opposite sides of the equator. (f) Scheme of the resulting chorus elements detected by the spacecraft on the left (upper) and right (lower) of the equator.

The considered event was used by Demekhov et al. (2017) for demonstrating the ability of the BWO model to reproduce both individual chorus elements and their sequence. We refer the reader to that paper for details of the simulation parameters.

Figures 3a and 3b show the dynamic spectra of the simulated VLF waves propagating in the positive s direction on the opposite sides from the geomagnetic equator, s being the coordinate along $\vec{B}_0$. It is clearly seen that the chorus elements are shifted to higher frequencies at ($s \simeq -1,100$ km), that is, where the waves propagate toward the equator, compared with $s \simeq +1,100$ km where the waves propagate from the equator. The amplitude of the waves propagating to the equator is 2–3 times lower than those propagating from the equator. This ratio is in quite a good agreement with the values observed at similar distances from the equator (see Figure S3 in the supporting information).

Figure 3c shows the dynamic spectrum of waves propagating in both directions at the point $|s| \approx 1,100$ km. This spectrum was obtained by performing simulations separately for waves (and their resonant electrons), which propagate in both directions, converting the obtained magnetic field amplitudes into Poynting fluxes and summing up the results. We assumed these subsystems to be independent, that is, neglect possible wave reflections and the effect of energetic electron bouncing, which can couple the oppositely propagating waves if the electrons preserve phase bunching after their mirror reflection.

The combined spectrum in Figure 3c shows more clearly the same features as Figures 3a and 3b, that is, that the simulated chorus waves propagating away from the magnetic equator have lower frequency and higher amplitude than the oppositely propagating waves.

4. Discussion

The observation and simulation results presented in sections 2 and 3.2, respectively, agree with each other and demonstrate an upward frequency shift of waves propagating toward the geomagnetic equator compared with those propagating away from the equator.

This shift can be qualitatively understood in terms of the evolution of the electron distribution function in the course of electron motion along the field line. A phenomenological model of such an evolution was suggested by Trakhtengerts et al. (2007) who described the shift of a hypothetical step in the distribution function along the velocity component parallel to B_0:

$$\frac{\mathrm{d}V_*}{\mathrm{d}t} \approx -\frac{\Omega_{\mathrm{tr}}^2}{2\pi k} - \frac{V_\perp^2 V_\parallel}{2V_* B_0}\,\frac{\mathrm{d}B_0}{\mathrm{d}s}\,. \tag{1}$$

Here, s is the direction along the geomagnetic field, V_* is the absolute value of the characteristic parallel velocity $V_\parallel$ corresponding to the particles generating the waves, $V_\perp$ is the perpendicular velocity, k is the wave number, and $\Omega_{tr} \simeq (ekV_\perp B/m)^{1/2}$ is the frequency of particle oscillations in the wavefield. In the latter formula, e and m are the elementary charge and electron mass, respectively, and B is the amplitude of the wave's magnetic field. Obviously, $V_\parallel \mathrm{d}B_0/\mathrm{d}s$ is the time derivative of B_0 in the resonant electron reference frame.

Equation (1) holds true not only for a step deformation in parallel velocities but also for any unstable feature of the electron distribution function in the velocity space, which generates large wave growth rates typical for chorus. The first term on the right-hand side of equation (1) describes the erosion of the unstable feature in the region of particle trapping by the wavefield (see Demekhov et al., 2017; Trakhtengerts & Rycroft, 2008 for detail), and the second term is due to the magnetic field inhomogeneity (magnetic mirror force). A decrease in V_* resulting from the nonlinear erosion corresponds, through the cyclotron resonance condition (e.g., Equation (4) in Demekhov et al., 2017) to an increase in the frequency of generated waves. As was shown in the above mentioned paper, the concept of erosion agrees well with that of electron hole formation described by Omura et al. (2008).

Equation (1) can (without considering amplitude variations) explain the spectral differences for chorus elements with the group velocities directed toward and away from the equator. The two terms on the right-hand side of equation (1) have the same signs for the former elements ($V_\parallel \mathrm{d}B_0/\mathrm{d}s > 0$ since the corresponding resonant electrons move away from the equator; see blue symbols on the sketch in Figure 3d) and opposite signs for the latter ones ($V_\parallel \mathrm{d}B_0/\mathrm{d}s < 0$, see red symbols in Figure 3d). Therefore, for the electrons moving to the equator the effect of magnetic field inhomogeneity partially compensates the nonlinear decrease in V_*. As a result, the elements propagating from the equator are generated by the electrons with much less distorted initial distribution function and higher parallel velocities and, therefore, start from lower frequencies.

A similar effect of mixing different Poynting flux directions in the chorus source region has been demonstrated using the wave data of the Cluster spacecraft (Santolík et al., 2004, 2008; Trakhtengerts et al., 2007), but the central position of the chorus source region was estimated from time averaged data, without the possibility of calculating the Poynting vector for individual chorus elements.

Figure 3e shows schematically the formation of chorus elements in space and time, based on the simulation results. Importantly, higher-frequency waves (f_5 and f_6) do not propagate to the opposite side of the equator and are damped along a short distance from their origin. This damping is a feature of our simulation and originates from highly nonlinear interaction with resonant electrons. It ensures the absence of

higher-frequency parts in chorus elements propagating away from the equator, as depicted in Figure 3f. Low frequencies do not experience this damping and are amplified also on their path toward the equator.

In our case, there is an uncertainty of B_0-minimum position for every specific case, since the TS05 model is statistical. We decrease this uncertainty by analyzing many events, which confirms case studies and is consistent with simulation results.

One can also notice in Figure 2d that most events with opposite Poynting flux directions were detected within a distance of 5,000 km from the model B_0-minimum, which is a typical scale of the chorus source region along the field line. This yields another indication that the B_0-minimum point has been correctly found for the majority of events.

Thus, the obvious similarities in observed and simulated spectra support the proposed mechanism of chorus frequency change depending on the propagation direction.

The observed difference in the amplitudes of oppositely propagating waves is also consistent with the simulation results and qualitative explanation. Indeed, the waves propagating from the equator have been amplified over much greater path including the central part of the source region.

Recall that Agapitov et al. (2011) proposed another explanation of the observed effect based on an outward shift of chorus waves during their propagation in the magnetosphere, reflection from lower hybrid resonance region, and coming back to the equatorial region. However, this mechanism would only explain the existence of weaker chorus at higher frequencies. It does not give preference to the waves propagating either to or from the equator, since the reflected waves would naturally continue their path from one side of the equator to the other.

One more possible explanation for the observed frequency difference of waves propagating in different directions could be related to nonlinear wave absorption at one half of the local gyrofrequency (Omura et al., 2009), which causes damping of slightly oblique waves at amplitudes above a certain threshold. Nonlinear attenuation of waves propagating in one direction (from the equator) could enable visibility of weaker waves propagating into the opposite direction (toward the equator), which are unaffected by nonlinear damping. However, the theory of this nonlinear damping has not yet been developed to a stage allowing one to determine the amplitude level below which the damping stops being effective. Therefore, one cannot say whether this mechanism can damp initially stronger waves propagating from the equator to a lower level than the weak oppositely propagating waves. Note also that such a mechanism could only act close to $0.5f_{c,e}$.

5. Conclusions

In summary, we have identified more than hundred chorus events observed by the THEMIS spacecraft in the vicinity of the geomagnetic equator and found a peculiar feature of their spectrum. Chorus elements with Poynting flux directed toward the equator have slightly higher frequencies and lower amplitudes than the elements detected at the same location but propagating away from the equator. The growth rates of oppositely propagating waves are the same, thus indicating their possible origin in the same flux tube. We demonstrated this feature for three example events and confirmed it statistically with 106 events from the years 2007–2012.

The observed feature was also demonstrated in self-consistent simulations based on the BWO model of chorus generation. It can be qualitatively explained in terms of a joint action of nonlinear processes deforming the distribution function under the action of the wavefield and the mirror force changing the parallel velocity of resonant particles.

The reported result demonstrates growing consistency between the existing theoretical and numerical models of chorus formation and detailed observations inside the wave generation region.

Acknowledgments
A. D. is grateful to the Russian Science Foundation for supporting his work under Grant 15–12–20005. U. T., M. H., and O. S. acknowledge support from the MEYS LTAUSA17070 project and from the Czech Academy of Sciences through the Praemium Academiae award. U. T., M. H., and O. S. acknowledge funding received from the European Union's Horizon 2020 research and innovation programme under Grant Agreement 870452 (PAGER). THEMIS data are available from the project site (https://sprg.ssl.berkeley.edu/data/themis/). We acknowledge NASA Contract NAS5-02099 and V. Angelopoulos for use of data from the THEMIS Mission. Specifically, J. W. Bonnell and F. S. Mozer for use of EFI data, C. W. Carlson and J. P. McFadden for use of ESA data, and A. Roux (in memoriam) and O. LeContel for use of SCM data.

References

Agapitov, O. V., Krasnoselskikh, V., Zaliznyak, Y., Angelopoulos, V., Le Contel, O., & Rolland, G. (2011). Observations and modeling of forward and reflected chorus waves captured by THEMIS. *Annales Geophysicae*, *29*(3), 541–550. https://doi.org/10.5194/angeo-29-541-2011

Angelopoulos, V. (2008). The THEMIS mission. *Space Science Reviews*, *141*(1-4), 5–34. https://doi.org/10.1007/s11214-008-9336-1

Auster, H. U., Glassmeier, K. H., Magnes, W., Aydogar, O., Baumjohann, W., Constantinescu, D., et al. (2008). The THEMIS fluxgate magnetometer. *Space Science Reviews*, *141*(1-4), 235–264. https://doi.org/10.1007/s11214-008-9365-9

Bonnell, J. W., Mozer, F. S., Delory, G. T., Hull, A. J., Ergun, R. E., Cully, C. M., et al. (2008). The electric field instrument (EFI) for THEMIS. *Space Science Reviews*, *141*(1-4), 303–341. https://doi.org/10.1007/s11214-008-9469-2

Breneman, A. W., Crew, A., Sample, J., Klumpar, D., Johnson, A., Agapitov, O., et al. (2017). Observations directly linking relativistic electron microbursts to whistler mode chorus: Van Allen Probes and FIREBIRD II. *Geophysical Research Letters*, *44*, 11,265–11,272. https://doi.org/10.1002/2017GL075001

Burtis, W. J., & Helliwell, R. A. (1975). Magnetospheric chorus: Amplitude and growth rate. *Journal of Geophysical Research*, *80*(22), 3265–3270. https://doi.org/10.1029/JA080i022p03265

Demekhov, A. G. (2011). On the generation of VLF emissions with increasing and decreasing frequency in the magnetospheric cyclotron maser in the backward-wave oscillator regime. *Radiophysics and Quantum Electronics*, *53*(11), 609–622.

Demekhov, A. G., Taubenschuss, U., & Santolík, O. (2017). Simulation of VLF chorus emissions in the magnetosphere and comparison with THEMIS spacecraft data. *Journal of Geophysical Research: Space Physics*, *122*(1), 166–184. https://doi.org/10.1002/2016JA023057

Demekhov, A. G., & Trakhtengerts, V. Y. (2005). Dynamics of the magnetospheric cyclotron ELF/VLF maser in the backward-wave -oscillator regime. I. Basic equations and results in the case of a uniform magnetic field. *Radiophysics and Quantum Electronics*, *48*(9), 639–649.

Demekhov, A. G., & Trakhtengerts, V. Y. (2008). Dynamics of the magnetospheric cyclotron ELF/VLF maser in the backward-wave -oscillator regime. II. Influence of the magnetic-field inhomogeneity. *Radiophysics and Quantum Electronics*, *51*(11), 880–889.

Hikishima, M., Yagitani, S., Omura, Y., & Nagano, I. (2009). Full particle simulation of whistler-mode rising chorus emissions in the magnetosphere. *Journal of Geophysical Research*, *114*, A01203. https://doi.org/10.1029/2008JA013625

Katoh, Y., & Omura, Y. (2006). Electron hybrid code simulation of whistler-mode chorus generation with real parameters in the Earth's inner magnetosphere. *Earth, Planets, and Space*, *68*(1), 192. https://doi.org/10.1186/s40623-016-0568-0

Kuzichev, I. V., Soto-Chavez, A. R., Park, J., Gerrard, A., & Spitkovsky, A. (2019). Magnetospheric chorus wave simulation with the TRISTAN-MP PIC code. *Physics of Plasmas*, *26*, 072,901. https://doi.org/10.1063/1.5096537

Le Contel, O., Roux, A., Robert, P., Coillot, C., Bouabdellah, A., de la Porte, B., et al. (2008). First results of the THEMIS search coil magnetometers. *Space Science Reviews*, *141*(1-4), 303–341. https://doi.org/10.1007/s11214-008-9469-2

LeDocq, M. J., Gurnett, D. A., & Hospodarsky, G. B. (1998). Chorus source locations from VLF Poynting flux measurements with the Polar spacecraft. *Geophysical Research Letters*, *25*(21), 4063–4066.

Lepping, R. P., Acũna, M. H., Burlaga, L. F., Farrell, W. M., Slavin, J. A., Schatten, K. H., et al. (1995). The WIND Magnetic Field Investigation. *Space Science Reviews*, *71*(1–4), 207–229.

Li, W., Thorne, R. M., Bortnik, J., Nishimura, Y., Angelopoulos, V., Chen, L., et al. (2010). Global distributions of suprathermal electrons observed on THEMIS and potential mechanisms for access into the plasmasphere. *Journal of Geophysical Research*, *115*, A00J10. https://doi.org/10.1029/2010JA015687

Lin, R. P., Anderson, K. A., Ashford, S., Carlson, C., Curtis, D., Ergun, R., et al. (1995). A three-dimensional plasma and energetic particle investigation for the Wind spacecraft. *Space Science Reviews*, *71*(1–4), 125–153.

McComas, D. J., Bame, S. J., Barker, P., Feldman, W. C., Phillips, J. L., Riley, P., & Griffee, J. W. (1998). Solar Wind Electron Proton Alpha Monitor (SWEPAM) for the Advanced Composition Explorer. *Space Science Reviews*, *86*(1–4), 563–612.

McFadden, J. P., Carlson, C. W., Larson, D., Ludlam, M., Abiad, R., Elliott, B., et al. (2008). The THEMIS ESA plasma instrument and in-flight calibration. *Space Science Reviews*, *141*(1-4), 277–302. https://doi.org/10.1007/s11214-008-9440-2

Nunn, D., & Omura, Y. (2012). A computational and theoretical analysis of falling frequency VLF emissions. *Journal of Geophysical Research*, *117*, A08228. https://doi.org/10.1029/2012JA017557

O'Brien, T. P., Lorentzen, K. R., Mann, I. R., Meredith, N. P., Blake, J. B., Fennell, J. F., et al. (2003). Energization of relativistic electrons in the presence of ULF power and MeV microbursts: Evidence for dual ULF and VLF acceleration. *Journal of Geophysical Research*, *108*(A8), 1329. https://doi.org/10.1029/2002JA009784

Oliven, M. N., & Gurnett, D. A. (1968). Microburst phenomena. 3. An association between microbursts and VLF chorus. *Journal of Geophysical Research*, *73*(7), 2355–2362. https://doi.org/10.1029/JA073i007p02355

Omura, Y., Hikishima, M., Katoh, Y., Summers, D., & Yagitani, S. (2009). Nonlinear mechanisms of lower-band and upper-band VLF chorus emissions in the magnetosphere. *Journal of Geophysical Research*, *114*, A07217. https://doi.org/10.1029/2009JA014206

Omura, Y., Katoh, Y., & Summers, D. (2008). Theory and simulation of the generation of whistler-mode chorus. *Journal of Geophysical Research*, *113*, A04223. https://doi.org/10.1029/2007JA012622

Parrot, M., Santolík, O., Gurnett, D. A., Pickett, J. S., & Cornilleau-Wehrlin, N. (2004). Characteristics of magnetospherically reflected chorus waves observed by CLUSTER. *Annals of Geophysics*, *22*, 2597–2606.

Reeves, G. D., Spence, H. E., Henderson, M. G., Morley, S. K., Friedel, R. H. W., Funsten, H. O., et al. (2013). Electron acceleration in the heart of the Van Allen radiation belts. *Science*, *341*(6149), 991–994. https://doi.org/10.1126/science.1237743

Roeder, J. L., Benbrook, J. R., Bering III, E. A., & Sheldon, W. R. (1985). X-ray microbursts and VLF chorus. *Journal of Geophysical Research*, *90*, 10,975–10,982. https://doi.org/10.1029/JA090iA11p10975

Santolík, O., Macusova, E., Titova, E. E., Kozelov, B. V., Gurnett, D., Pickett, J. S., et al. (2008). Frequencies of wave packets of whistler-mode chorus inside its source region: A case study. *Annales Geophysicae*, *26*(6), 1665–1670.

Santolík, O., Parrot, M., & Lefeuvre, F. (2003). Singular value decomposition methods for wave propagation analysis. *Radio Science*, *38*(1), 1010. https://doi.org/10.1029/2002JA009791

Santolík, O., Pickett, J. S., Gurnett, D. A., Menietti, J. D., Tsurutani, B. T., & Verkhoglyadova, O. (2010). Survey of Poynting flux of whistler mode chorus in the outer zone. *Journal of Geophysical Research*, *115*, A00F13. https://doi.org/10.1029/2009JA014925

Santolík, O., Gurnett, D. A., Pickett, J. S., Parrot, M., & Cornilleau-Wehrlin, N. (2004). A microscopic and nanoscopic view of storm-time chorus on 31 March 2001. *Geophysical Research Letters*, *31*, L02801. https://doi.org/10.1029/2003GL018757

Santolík, O., Gurnett, D. A., Pickett, J. S., Parrot, M., & Cornilleau-Wehrlin, N. (2005). Central position of the source region of storm–time chorus. *Planetary and Space Science*, *53*(1–3), 299–305.

Sazhin, S. S., & Titova, E. E. (1978). Dynamics of VLF chorus spectrum according to Lovozero station data. *Cosmic Research*, *15*(5), 684–685.

Smith, C. W., L'Heureux, J., Ness, N. F., Acuña, M. H., Burlaga, L. F., & Scheifele, J. (1998). The ACE Magnetic Fields Experiment. *Space Science Reviews*, *86*(1–4), 613–632.

Tao, X., Lu, Q., Wang, S., & Dai, L. (2014). Effects of magnetic field configuration on the day-night asymmetry of chorus occurrence rate: A numerical study. *Geophysical Research Letters*, *41*, 6577–6582. https://doi.org/10.1002/2014GL061493

Taubenschuss, U., Demekhov, A. G., & Santolík, O. (2017). Interpretation of whistler mode chorus observations with the backward wave oscillator model. In G. Fischer, G. Mann, M. Panchenko, & P. Zarka, (Eds.), *Planetary radio emissions viii, proceedings of the 8th international workshop held at seggauberg, austria, october 25-27, 2016* (pp. 233–242). Vienna: Austrian Academy of Sciences Press. https://doi.org/10.1553/PRE8s233

Taubenschuss, U., & Santolík, O. (2019). Wave polarization analyzed by singular value decomposition of the spectral matrix in the presence of noise. *Surveys in Geophysics*, *40*, 39–69. https://doi.org/10.1007/s10712-018-9496-9

Taubenschuss, U., Santolík, O., Breuillard, H., Li, W., & Le Contel, O. (2016). Poynting vector and wave vector directions of equatorial chorus. *Journal of Geophysical Research: Space Physics*, *121*, 11,912–11,928. https://doi.org/10.1002/2016JA023389

Taylor, W. W. L., & Gurnett, D. A. (1968). Morphology of VLF emissions observed with the Injun 3 satellite. *Journal of Geophysical Research*, *17*, 5615–5626. https://doi.org/10.1029/JA073i017p05615

Titova, E. E., Kozelov, B. V., Jiricek, F., Smilauer, J., Demekhov, A. G., & Trakhtengerts, V. Y. (2003). Verification of backwards wave oscillator model of VLF chorus generation using data from MAGION 5 satellite. *Annales Geophysicae*, *21*(5), 1073–1081.

Trakhtengerts, V. Y. (1995). Magnetosphere cyclotron maser: Backward wave oscillator generation regime. *Journal of Geophysical Research*, *100*(9), 17,205–17,210. https://doi.org/10.1029/95JA00843

Trakhtengerts, V. Y. (1999). A generation mechanism for chorus emission. *Annales Geophysicae*, *17*(1), 95–100.

Trakhtengerts, V. Y., Demekhov, A. G., Titova, E. E., Kozelov, B. V., Santolik, O., Gurnett, D., & Parrot, M. (2004). Interpretation of Cluster data on chorus emissions using the backward wave oscillator model. *Physics of Plasmas*, *11*(4), 1345–1351.

Trakhtengerts, V. Y., Demekhov, A. G., Titova, E. E., Kozelov, B. V., Santolik, O., Macusova, E., et al. (2007). Formation of VLF chorus frequency spectrum: Cluster data and comparison with the backward wave oscillator model. *Geophysical Research Letters*, *34*, L02104. https://doi.org/10.1029/2006GL027953

Trakhtengerts, V. Y., & Rycroft, M. J. (2008). *Whistler and Alfvén mode cyclotron masers in space*. New York: Cambridge University Press.

Tsurutani, B. T., & Smith, E. J. (1977). Two types of magnetospheric ELF chorus and their substorm dependences. *Journal of Geophysical Research*, *82*, 5112–5128.

Tsyganenko, N. A., & Sitnov, M. I. (2005). Modeling the dynamics of the inner magnetosphere during strong geomagnetic storms. *Journal of Geophysical Research*, *110*, A03208. https://doi.org/10.1029/2004JA010798